A granular medium model for liquefaction analysis of sands*
砂土液化分析的散粒体模型

Shen Zhujiang (沈珠江)
(Nanjing Hydraulic Research Institute, Nanjing, 210024)

Abstract In this paper the main achievements gained from the study on the change of sand texture during its deformation are summarized first, and then an incrementally nonlinear model different from the existing elasto-plastic ones is presented. In the formulation of this model both the reversible and the irreversible deformation due to the change of mean normal stress and normalized shear stress, the turn of stress path and the rotation of principal stress axis have been taken into account. The computed examples show that the proposed model can successfully simulate the softening of dense sand due to dilatancy and the undrained instability of loose sand under monotonous loading, the accumulation of residual strain and pore pressure during repeated loading and also the liquefaction induced by the change of Lode's angle and the rotation of principal stress axis.

Key words Sand liquefaction, constitutive model, granular medium

Shen Zhujiang Born in Jan. 1933, male, member of Chinese Academy of Science, professor of Geotechnical Engineering Department, Nanjing Hydraulic Research Institute.

文 摘 在归纳砂土组构张量研究成果的基础上提出一个与已有弹塑性模型不同的新的增量非线性模型。该模型全面地考虑了平均压应力、归一化剪应力、Lode 角和主应力轴变化所引起的可逆和不可逆的变形,成功地模拟了单调荷载下密砂的剪胀软化和松砂的不排水剪切失稳现象,往复荷载下的残余变形和孔隙压力积累以及 Lode 角和主应力轴变化下的液化现象。

关键词 砂土液化,本构模型,散粒体
中图法分类号 TU 435

1 Introduction*

The simulation of sand liquefaction is one of most challenging tasks in the soil mechanics. Dozens of constitutive models for this purpose have been proposed. Despite of that among them significant contributions have been made by some authors in the understanding of soil behavior during cyclic loading[1~5], but none of them can be considered as fully satisfactory. It is the writer's opinion that all these model do not totally free of the basic framework of traditional soil plasticity consisted of yield function and plastic potential, although the hypoplastic type of model has already postulated that the direction of plastic deformation dependent on both the direction of total stress and the direction of stress increment. At the same time, many experimental findings have already highlight the mechanism of plastic deformation[6~8], and some authors tried to take it into account in the formulation of constitutive model[9], but no successful results in the modeling of soil behavior based on the understanding of the mechanism of plastic deformation has been reported. In the following a macroscopic model will be suggested on the basis of these microscopic findings.

2 Basic assumption

A granular medium is assumed to have following characteristics:

(1) No bonding exist between particles and the particles are strong enough to avoid breakage;

(2) Both sliding and rolling between particles have their contribution in the plastic deformation, and the sliding between particles obeys Coulomb's friction law;

(3) An assembly of particles can be described by two internal tensor variables ——contact tensor and orientation tensor[10].

The variation of these two tensors during the process of loading is the key point in the understanding of mechanism of plastic deformation of soils. Based on the experimental findings following laws for describing the change of internal variables are postulated:

①Densification law ——The spherical part of contact tensor is characterized by the coordination number which is proportional with the density of sand and an isotropic hardening will take place during densification;

②Homogenization law ——During densification the large pores reduce their volume first while the small pores remain essentially unchanged, therefore the distribution of void ratio becomes more uniform (Fig. 1), this process offers an additional reason of isotropic hardening;

③Co-axis law ——The principal axis of contact tensor is always coincident with the principal axis of stress tensor (Fig. 2(c));

④Proportion law ——The deviatoric part of contact tensor is proportional with the deviatoric part of stress tensor and the degree of anisotropic hardening is proportional with the principal stress ratio (Fig. 2(b));

⑤Orientation law ——Less volume will be occupied when the ellipsoid particles are parallelly piled up, therefore the orientation ratio (ratio of longer axis to shorter axis of orientation tensor) should increase during plastic deformation (Fig. 3(b));

⑥Limit rotation law ——The axis of orientation tensor is formed during the deposition of particles and can be undergone only limit rotation to make its longer axis of particle to be parallel with the direction of maximum shear stress (Fig. 3(c)).

Some consequences can be drown from these microscopic laws:

* Supported by Chinese National Science Foundation(No. 19772019)
Received June 1, 1999

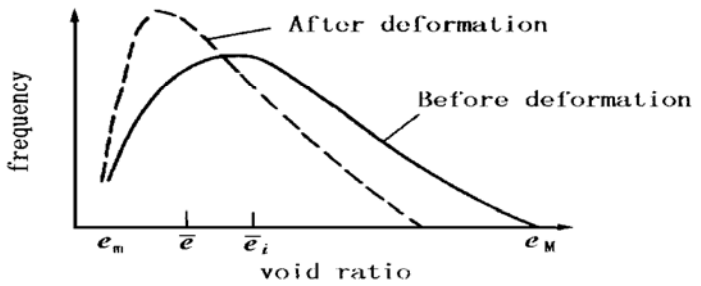

Fig. 1 Pore distribution

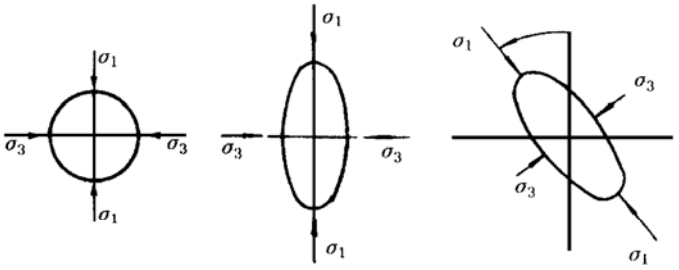

(a) $\sigma_1 = \sigma_3$ (b) $\sigma_1 > \sigma_3$ (c) Rotation of axis

Fig. 2 Change of contact tensor

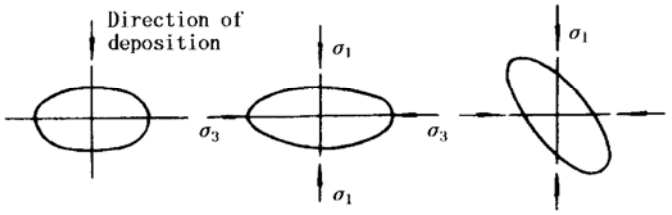

(a) Before loading (b) After loading (c) In the shear band

Fig. 3 Change of orientation tensor

①Failure of flow theory of plasticity ——Because the rolling of particles is determined by the stress increment and the sliding only obeys the flow law, the direction of plastic strain increment must be dependent upon both the direction of total stress and the direction of stress increment, as shown in Fig. 4;

②Reversibility of dilatant strain ——Dilation is associated with positive angle of contact relative to shear direction and the amount of positively oriented contacts increases with the increase of principal stress ratio, but once the shear direction is reversed the original positively oriented contacts change to be negatively oriented and a negative dilatancy takes place (Fig. 5);

③Mechanism of isotropic hardening ——Hardening is the result of increase of number of contacts. Densification means the increase of contact number in all direction and causes an isotropic hardening, it is an irrecoverable process according to the second law of thermodynamics when soil is under confined condition. Of cause dilation can induce some amount of softening, but it is only a temporary phenomena due to the reversibility of dilatant strain;

④Mechanism of anisotropic hardening ——Anisotropic hardening happens only in the direction perpendicular to the major principal stress, while in the direction perpendicular to the minor principal axis, the contact number decreases. The conditions of loss of contact to cause anisotropic hardening under 3 different types of loading can be explained through the three-particle model as shown in Fig. 6, where symbol / means the loss of a contact and μ is the angle of surface friction between particles.

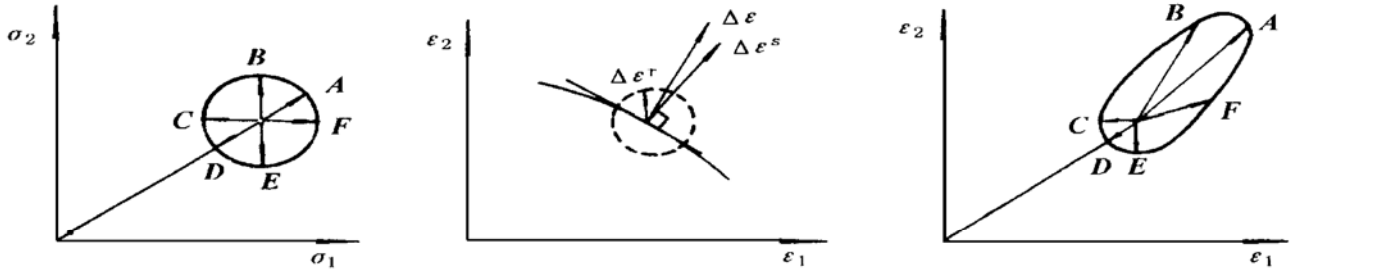

(a) Stress increments (b) Strain increments (c) Composed strain increments

Fig. 4 Plastic deformation due to particle rolling and sliding

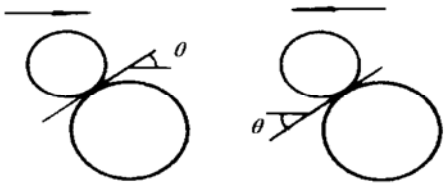

Fig. 5 Positive and negative dilatancy

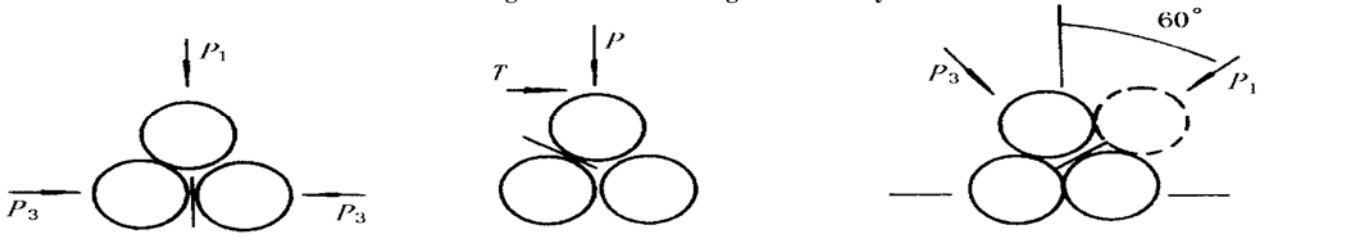

$P_1 / P_3 = \cot(30^\circ - \mu)$ (a) Compression

$T / P = \tan(30^\circ + \mu)$ (b) Shearing

$P_1 / P_3 = \cot(30^\circ - \mu)$ (c) Rotation of stress axia

Fig. 6 Three-particle model

3 Formulation of constitutive equations

3.1 Initial loading

The proposed model will be formulated based on following relationships:

①Logarithmic function for compression under constant η

$$e = e_0 - c_c \lg \frac{p}{p_0} \tag{1}$$

②Hyperbolic function for shearing under constant p

$$\varepsilon_{sd} = \frac{ar}{1-r} \tag{2}$$

③Linear function for dilatancy

$$\frac{\Delta\varepsilon_{vd}}{\Delta\varepsilon_{sd}} = \frac{1}{\lambda}(\eta_d - \eta) \tag{3}$$

In above-mentioned equations, $r = \eta/\eta_f$, $\eta = \frac{1}{\sqrt{2}}\left[\left|\frac{\sigma_1-\sigma_2}{\sigma_1+\sigma_2}\right|^2 + \left|\frac{\sigma_2-\sigma_3}{\sigma_2+\sigma_3}\right|^2 + \left|\frac{\sigma_3-\sigma_1}{\sigma_3+\sigma_1}\right|^2\right]^{1/2}$, $\eta_f = \sin\varphi$, $p = \frac{1}{3}(\sigma_1+\sigma_2+\sigma_3)$, $\varepsilon_v = \varepsilon_1+\varepsilon_2+\varepsilon_3$, $\varepsilon_s = \frac{1}{\sqrt{2}}[(\varepsilon_1-\varepsilon_2)^2+(\varepsilon_2-\varepsilon_3)^2+(\varepsilon_3-\varepsilon_1)^2]^{1/2}$. r can be named as mobilization ratio and η is normalized shear stress. λ and η_d are 2 constants. c_c and a are functions of void ratio or volumetric strain. The η = const. curves in the deviatoric plane are shown in Fig. 7.

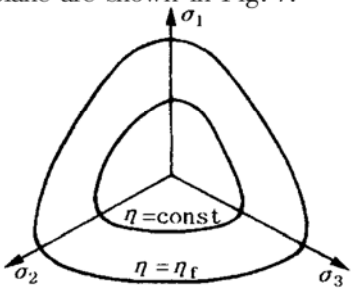

Fig. 7 Failure criterion in π plane

From Eq. (1) the increments of volumetric and shear deformation due to compression will be respectively as follows

$$\Delta\varepsilon_{vc} = C_c \frac{\Delta p}{p} \tag{4a}$$

$$\Delta\varepsilon_{sc} = C_c \frac{\eta}{\eta_0}\frac{\Delta p}{p} \tag{4b}$$

where $C_c = \frac{0.434c_c}{1+e_0}$, $\eta_0 = \frac{1-K_0}{1+K_0}$ is η value under one-dimensional compression, K_0 is coefficient of earth pressure at rest, because in this case $\Delta\varepsilon_2 = \Delta\varepsilon_3 = 0$, $\Delta\varepsilon_v = \Delta\varepsilon_s = \Delta\varepsilon_1$. If η_f is a linear function of volumetric strain as

$$\eta_f = \eta_{f0} + c_f \varepsilon_v \tag{5}$$

then from Eqs. (2) and (5)

$$\Delta\varepsilon_{sd} = \frac{a}{(1-r)^2}\left(\Delta r - \frac{c_f r}{\eta_f}\frac{\partial\varepsilon_{vd}}{\partial\varepsilon_{sd}}\Delta\varepsilon_{sd}\right) \tag{6}$$

or after substitution of Eq. (3)

$$\Delta\varepsilon_{vd} = \frac{a(\eta_d-\eta)}{\lambda g}\Delta r \tag{7a}$$

$$\Delta\varepsilon_{sd} = \frac{a}{g}\Delta r \tag{7b}$$

where $\Delta r = \Delta\eta/\eta_f$ and

$$g = (1-r)^2 + c_f\frac{ar}{\eta_f}\frac{\eta_d-\eta}{\lambda} \tag{8}$$

When $r \to 1$ and $\eta \geqslant \eta_d$, g may become negative, therefore a strain softening can be simulated. The total increment of volumetric deformation and total increment of shear deformation will be as follows respectively

$$\Delta\varepsilon_v = C_c\frac{\Delta p}{p} + \frac{a(\eta_d-\eta)}{\lambda g}\Delta r \tag{9a}$$

$$\Delta\varepsilon_s = C_c\frac{\eta}{\eta_0}\frac{\Delta p}{p} + \frac{a}{g}\Delta r \tag{9b}$$

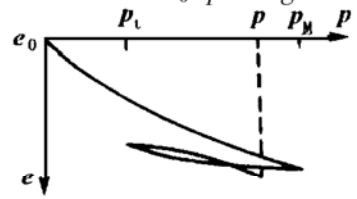

Fig. 8 Turn of stress path in compression

3.2 Complex loading

(1) Separation of elastic and plastic deformation

Experimental results show that even within small strain range ($< 10^{-4}$), the stress strain curve is still nonlinear. Therefore, if there exist elastic deformation, it must be negligibly small. However, according to the theory of dual origination of plastic deformation, some amount of plastic deformation originated from particle rolling have similar behavior as elastic deformation, and hereafter will be called as quasi-elastic deformation. In addition, as mentioned before, the dilatant part of volumetric deformation is recoverable. and can be also regarded as a kind of quasi-elastic deformation. If c_s is swelling index as usually used, the quasi-elastic part and plastic part of volumetric strain can be written separately as follows

$$\Delta\varepsilon_v^e = C_s\frac{\Delta p}{p} - \frac{a\eta}{\lambda g}\Delta r \tag{10a}$$

$$\Delta\varepsilon_v^p = (C_c - C_s)\frac{\Delta p}{p} + \frac{a\eta_d}{\lambda g}\Delta r \tag{10b}$$

where $C_s = \frac{0.434c_s}{1+e_0}$

The corresponding quasi-elastic and plastic component of deviatoric deformation will be

$$\Delta\varepsilon_s^e = C_s\frac{\eta}{\eta_0}\frac{\Delta p}{p} + w\frac{a}{g}\Delta r \tag{11a}$$

$$\Delta\varepsilon_s^p = (C_c - C_s)\frac{\eta}{\eta_0}\frac{\Delta p}{p} + (1-w)\frac{a}{g}\Delta r \tag{11b}$$

where w is a weight function of quasi-elastic deformation among the total deformation due to shearing. It can be assumed that the part of shear deformation originated from particle sliding increases rapidly when $\eta \to \eta_f$, but the another part originated from particle rolling does not. Therefore we can assume $w = g$, and Eqs. (11a) and (11b) can be rewritten as

$$\Delta\varepsilon_s^e = C_s\frac{\eta}{\eta_0}\frac{\Delta p}{p} + a\Delta r \tag{12a}$$

$$\Delta\varepsilon_s^p = (C_c - C_s)\frac{\eta}{\eta_0}\frac{\Delta p}{p} + a\frac{1-g}{g}\Delta r \tag{12b}$$

(2) Turn of stress path

The above-derived equation is applicable only for initial loading. For the case of turn of stress path following equations for plastic volumetric and deviatoric deformation can be suggested

$$\Delta\varepsilon_v^p = (C_c - C_s)\frac{p^*}{p_f}\frac{\Delta p}{p} + \frac{a\eta_d}{\lambda g^*}\Delta r^* \tag{13a}$$

$$\Delta\varepsilon_s^p = (C_c - C_s)\frac{\eta}{\eta_0}\frac{p^*}{p_f}\frac{\Delta p}{p} + a\frac{1-g^*}{g^*}\Delta r^* \tag{13b}$$

where $\Delta r^* = \Delta\eta^*/\eta_f^*$ and

$$g^* = (1-r^*)^2 + c_f\frac{ar^*}{\eta_f^*}\frac{\eta_d - \eta}{\lambda} \tag{14}$$

$$p^* = |p - p_t| \tag{15}$$

$$p_f = p_M - \mathrm{sign}(p - p_t)p_t \tag{16}$$

$$\eta^* = \sqrt{\eta^2 - 2\eta\eta_t\cos(\rho - \rho_t) + \eta_t^2} + \eta_t\cos\frac{\delta}{2} \tag{17}$$

$$\eta_f^* = \sqrt{\eta_f^2 - 2\eta_f\eta_t\cos(\rho - \rho_t) + \eta_t^2} + \eta_t\cos\frac{\delta}{2} \tag{18}$$

In aforegoing equations p_t and η_t are values of p and η at the turning point, p_M is the maximum pressure in the loading history (Fig. 8), δ is the turning angle, ρ, ρ_t and ρ_f are Lode's angles of present stress, stress at turning point and stress at failure state respectively (Fig. 9(a)). The late one is determined by solving following equation

$$\rho_f = \rho_t + \delta - \arcsin\left(\frac{\eta_t}{\eta_f}\sin\delta\right) \tag{19}$$

From Eq. (17)

$$\Delta\eta^* = C_a\Delta\eta + C_t\Delta\rho \tag{20}$$

where $C_a = [\eta - \eta_t\cos(\rho - \rho_t)]/\bar{\eta}$, $C_t = \eta\eta_t\sin(\rho - \rho_t)/\bar{\eta}$, and $\bar{\eta} = \sqrt{\eta^2 - 2\eta\eta_t\cos(\rho - \rho_t) + \eta_t^2}$. Eqs (17) and (20) satisfy following conditions

for initial loading

$\delta = 0°$, $\rho - \rho_t = 0$: $\eta^* = \eta$, $\Delta\eta^* = \Delta\eta$

for unloading and repeated loading

$\delta = 180°$, $\rho - \rho_t = 0$: $\eta^* = \eta_t - \eta$, $\Delta\eta^* = |\Delta\eta|$

$\delta = 180°$, $\rho - \rho_t = 180$: $\eta^* = \eta_t + \eta$, $\Delta\eta^* = \Delta\eta$

In the case of continuously rotating stress path under constant η, $\delta = 90°$, $\rho = \rho_t$, then

$$\eta^* = \eta_t\cos45° \tag{17a}$$

$$\Delta\eta = \eta_t\Delta\rho \tag{20a}$$

In the above-mentioned formulation no unloading criterion has been introduced. But some thing like unloading takes place when turning angle of stress path $\delta = 180°$, because in this case $p^* = 0$, $\eta^* = 0$, and $r^* = 0$, therefore $\Delta\varepsilon_s^p = 0$, and in Eq. (13a) only the second term remains, i. e.

$$\Delta\varepsilon_v^p = \frac{a\eta_d}{\lambda}\Delta r^* \tag{21}$$

if the term containing c_f in Eq. (14) is neglected. Because $\Delta\eta^*$ is always positive, the volumetric contraction can take place at stress reverse accompanying with quasi-elastic deformation.

(3) Isotropic hardening

To take account of isotropic hardening during repeated loading, c_c and a are assumed to be two variables as follows

$$c_c = c_{c0}\exp(-b\cdot\xi) \tag{22a}$$

$$a = a_0\exp(-d\cdot\xi) \tag{22b}$$

where $\xi = \int|d\varepsilon_s|$ is the accumulated value of shear strain, it is taken as a measure of void ratio homogenization. c_{c0}, a_0, b and d are 4 constants.

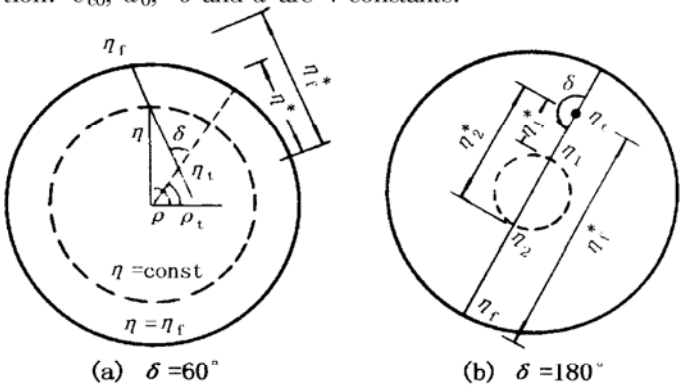

Fig. 9　Rotation of stress path in π plane

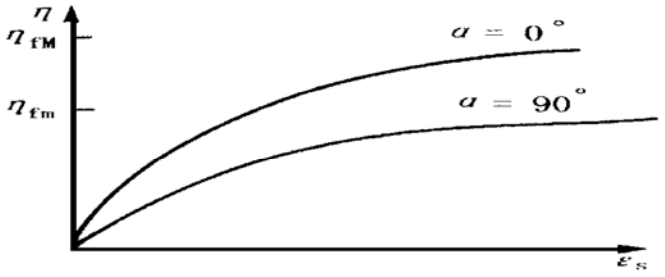

Fig. 10　Anisotropic shear strength

(4) Rotation of principal stress axis

Fig. 6(c) clearly explains the mechanism of plastic deformation induced by rotation of stress axis. Now we should find an expression similar to Eq. (20a). If we recognize that the effect of rotation of stress axis in 90° is equivalent to the change of stress state from compression test to extension test with increase of Lode's angle in 60°, then the following expression can be postulated for a rotation of stress axis $\Delta\alpha$

$$\Delta\eta^* = \frac{2}{3}\eta\Delta\alpha \tag{23}$$

However, there must be another mechanism for real soils due to their anisotropic nature gained from particle orientation. Therefore the assumption of constant η_f until now used must be abandoned. From experimental results of many authors[11], following expression for the variation of η_f with the change of principal axis will be adopted

$$\eta_f = \frac{1}{2}(\eta_{fM} + \eta_{fm}) + \frac{1}{2}(\eta_{fM} - \eta_{fm})\cos\alpha \tag{24}$$

where η_{fM} is the maximum value of η_f when $\alpha = 0°$, i. e. σ_1 axis coincides with the direction of deposition, η_{fm} is its minimum value when σ_1 axis rotates around 90° (Fig. 10). From Eqs. (23) and (24) the expression for increment of r will be

$$\Delta r^* = \frac{1}{\eta_f^*}(C_b|\Delta\alpha| + C_r^*\langle\Delta\alpha\rangle) \tag{25}$$

where $C_b = 2\eta/3$ and

$$C_r^* = \frac{\eta_{fM} - \eta_{fm}}{2\eta_f^*}\sin\alpha \tag{26}$$

This equation suggests that the rotation of stress in any direction may induce plastic deformation accompanying with the change of contact tensor, but the Macauley symbol $\langle\ \rangle$ means that plastic deformation due to change of orientation tensor can take place only when α increases from 0° to 90°. However, for quasi-elastic deformation both positive and negative value of $\Delta\alpha$must be taken into account, and Eqs. (25) and (26) can be rewritten as

$$\Delta r = \frac{1}{\eta_f}(\Delta\eta + C_r\Delta\alpha) \tag{25a}$$

where

$$C_r = \frac{\eta_{fM} - \eta_{fm}}{2\eta_f}\sin\alpha \tag{26a}$$

3.3 Final expressions

(1) Direction of strain increment

As mentioned above the quasi-elastic component of strain can be described by deformation theory of plasticity, the direction of its increment can be assumed as parallel to the direction of stress increment $\Delta S_{ij}/\Delta q$, where S_{ij} is deviatoric component of stress tensor, $\Delta q = \frac{1}{\sqrt{2}}[(\Delta\sigma_1 - \Delta\sigma_2)^2 + (\Delta\sigma_2 - \Delta\sigma_3)^2 + (\Delta\sigma_3 - \Delta\sigma_1)^2]^{1/2}$. Therefore, form Eqs. (10a) and (25a)

$$\Delta\varepsilon_v^e = C_s\frac{\Delta p}{p} - \frac{ar}{\lambda g}(\Delta\eta + C_r\Delta\alpha) \tag{27a}$$

$$\Delta e_{ij}^e = \left[C_s\frac{\eta}{\eta_0}\frac{\Delta p}{p} + \frac{a}{\eta_f}(\Delta\eta + C_r\Delta\alpha)\right]\frac{\Delta S_{ij}}{\Delta q} \tag{27b}$$

The flow theory of plasticity will be used to describe the remaining part of strain, i. e. its direction is parallel with the direction of normal of potential function $\eta = $ const. The corresponding equations will be

$$\Delta\varepsilon_v^p = (C_c - C_s)\frac{p^*}{p_f}\frac{\Delta p}{p} + \frac{a\eta_d}{\lambda g^*\eta_f^*}(C_a\Delta\eta + C_t\Delta\rho + C_b|\Delta\alpha| + C_r^*\langle\Delta\alpha\rangle) \tag{28a}$$

$$\Delta e_{ij}^p = \left[(C_c - C_s)\frac{\eta}{\eta_0}\frac{p^*}{p_f}\frac{\Delta p}{p} + a\frac{1 - g^*}{g^*\eta_f^*}\times(C_a\Delta\eta + C_t\Delta\rho + C_b|\Delta\alpha| + C_r^*\langle\Delta\alpha\rangle)\right]\frac{1}{N}\frac{\partial\eta}{\partial S_{ij}} \tag{28b}$$

where $N = \left[\frac{\partial\eta}{\partial S_{ij}}\cdot\frac{\partial\eta}{\partial S_{ij}}\right]^{1/2}$.

(2) Final expressions for strain increment

Because $\Delta\varepsilon_{ij} = \frac{1}{3}\Delta\varepsilon_v\delta_{ij} + \Delta e_{ij}$, δ_{ij} is unit tensor, summarizing the afore going equations yields

$$\Delta\varepsilon_{ij} = C_{ijkl}\Delta\sigma_{kl} \tag{29}$$

where

$$C_{ijkl} = A_1\delta_{ij}\frac{\partial p}{\partial\sigma_{kl}} - A_2\delta_{ij}\frac{\partial\eta}{\partial\sigma_{kl}} - A_2C_r\delta_{ij}\frac{\partial\alpha}{\partial\sigma_{kl}} + 3A_1n_{ij}\frac{\partial p}{\partial\sigma_{kl}} + \frac{a}{\eta_f}n_{ij}\frac{\partial\eta}{\partial\sigma_{kl}} + \frac{a}{\eta_f}C_rn_{ij}\frac{\partial\alpha}{\partial\sigma_{kl}} + A_3\delta_{ij}\frac{\partial p}{\partial\sigma_{kl}} + A_4C_a\delta_{ij}\frac{\partial\eta}{\partial\sigma_{kl}} + A_4C_t\delta_{ij}\frac{\partial\rho}{\partial\sigma_{kl}} + A_4(C_b + C_r^*)\delta_{ij}\frac{\partial\alpha}{\partial\sigma_{kl}} + 3A_3\frac{\eta_p^*}{\eta_0p_M}n_{ij}^* + A_5C_an_{ij}^*\frac{\partial\eta}{\partial\sigma_{kl}} + A_5C_tn_{ij}^*\frac{\partial\rho}{\partial\sigma_{kl}} + A_5(C_b + C_r^*)n_{ij}^*\frac{\partial\alpha}{\partial\sigma_{kl}} \tag{30}$$

where $A_1 = C_s/3p$; $A_2 = ar/\lambda g$; $A_3 = (C_c - C_s)/3p$; $A_4 = a\eta_d/3\lambda g\eta_f^*$; $A_5 = a(1 - g^*)/g^*\eta_f^*$ and $n_{ij} = \Delta S_{ij}/\Delta q$; $n_{ij}^* = \partial\eta^*/\partial S_{ij}$. Eq. (30) shows clearly 4 mechanisms of deformation, i. e. ① compression Δp, ② shearing $\Delta\eta$, ③ change of Lode's angle $\Delta\rho$ and ④ rotation of stress axis $\Delta\alpha$.

(3) Final expression for stress increment

Eq. (27) can be written shortly as

$$\Delta\varepsilon_v^e = \frac{1}{3K}\Delta p; \quad \Delta e_{ij}^e = \frac{1}{2G}\Delta S_{ij} \tag{31}$$

where

$$\frac{1}{K} = \frac{C_s}{p} - \frac{ar}{\lambda g}\frac{\Delta\eta + C_r\Delta\alpha}{\Delta p};$$
$$\frac{1}{2G} = \frac{C_s\eta}{p\eta_0}\frac{\Delta p}{\Delta q} + \frac{a}{\eta_f}\frac{\Delta\eta + C_r\Delta\alpha}{\Delta q} \tag{32}$$

K and G are bulk and shear modules in conventional mean, but they are apparently dependent on stress path. Then the inverse form of Eq. (31) will be

$$\Delta\sigma_{ij} = D_{ijkl}^{-1}\Delta\varepsilon_{ij}^e \tag{33}$$

Now Eq. (28) is shortly expressed by

$$\Delta\varepsilon_{ij}^p = C_{ijkl}^p\Delta\sigma_{kl} \tag{34}$$

We can get final expression by substituting $\Delta\varepsilon_{ij}^e = \Delta\varepsilon_{ij} - \Delta\varepsilon_{ij}^p$ into Eq. (33)

$$\Delta\sigma_{ij} = (I_{ijmn} + D_{ijkl}C_{klmn}^p)^{-1}D_{mnkl}\Delta\varepsilon_{kl} \tag{35}$$

where I_{ijkl} is unit tensor of fourth order.

(4) Expression for pore pressure

Under undrained condition, $\Delta\varepsilon_v = \Delta\varepsilon_v^e + \Delta\varepsilon_v^p = 0$, the pore pressure rise will be $\Delta u = -\Delta p$, and from Eqs. (27a) and (28a) we can obtain

$$\Delta u = \frac{K_u}{B}\Delta\varepsilon_{vd} \tag{36}$$

where

$$B = 1 + \frac{C_c - C_s}{C_s}\frac{p^*}{p_f} \tag{37}$$

$$\Delta\varepsilon_{vd} = \frac{a\eta_d}{\lambda g^*\eta_f^*}(C_a\Delta\eta + C_t\Delta\rho + C_b|\Delta\alpha| + C_r^*\langle\Delta\alpha\rangle) - \frac{a\eta}{\lambda g\eta_f}(\Delta\eta + C_r\Delta\alpha) \tag{38}$$

is the volumetric strain due to dilatancy, and

$$K_u = \frac{p}{C_s} \tag{39}$$

is rebound bulk modules as usually meaning.

4 Performance of model

To confirm the ability of the proposed model to simulate the deformation behavior under various loading conditions, a series of computed examples is presented in the following. In these computations following set of model constant derived from the conventional odometer test and triaxial compression test conducted on Fujian sand samples prepared with relative density of 50% is used: $c_{c0} =$

0.0048, c_s = 0.0086, a_0 = 0.0023, λ = 0.6, η_d = 0.45, η_f = 0.62. Another 3 constants b = 1.0, d = 2.0 and c_f = 1.5 are tentatively presumed. However, for a more dense sand η_d = 0.37 and η_f = 0.70 are assumed, and for a much more loose sand another pair of constants η_d = 0.65 and η_f = 0.58 is adopted.

4.1 Monotonous loading

For the case of conventional drained triaxial compression test the computed stress – strain curves for samples with different density are shown in Fig. 11. It can be seen that the strain softening behavior for medium and dense sand is properly simulated. Fig. 12 shows the corresponding curves under undrained state. In this case instead of volumetric strain the pore pressure build-up and the instability phenomenon with nearly complete liquefaction for loose sand are captured, but for medium sand after a flat section a rapid increase of deviatoric stress happens accompanying with decrease of pore pressure. Therefore the proposed model can properly simulate the drained and undrained behaviors of sands with different density by revising only two parameters η_d and η_f.

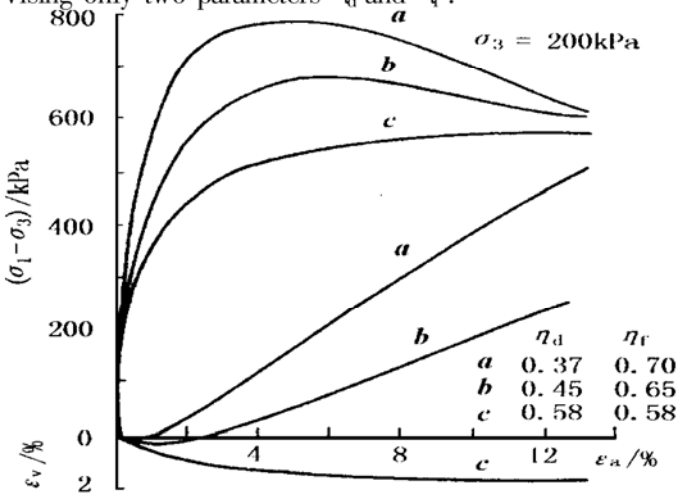

Fig. 11 Drained triaxial test

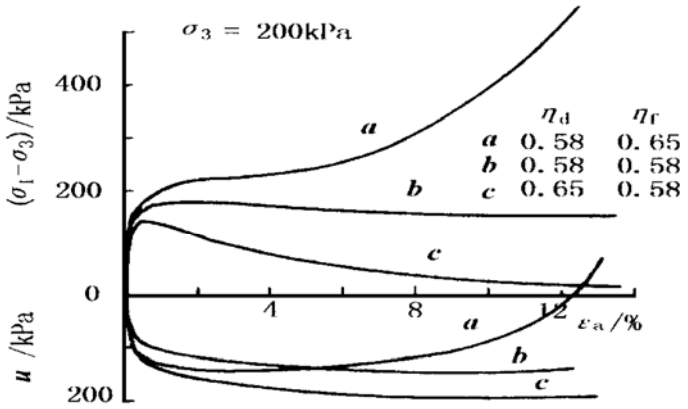

Fig. 12 Undrained triaxial test

4.2 Repeated loading

The computed results of one-dimensional repeated loading is shown in Fig. 13. Loops of stress – strain curves and accumulation of residual volumetric strain accompanying with gradual increase of lateral stress are fairly captured. The tendency of increase of volumetric strain and lateral stress will slow down more rapidly if larger values of model parameters b and d are used. In Fig. 14 one-way repeated triaxial compression test is simulated. The process of accumulation of axial strain and volumetric strain is also well reproduced. Finally, the conventional undrained cyclic triaxial test is simulated as shown in Fig. 15. The rapid increase of pore pressure at the stress reverse when $\eta \geqslant \eta_d$ is quite apparent.

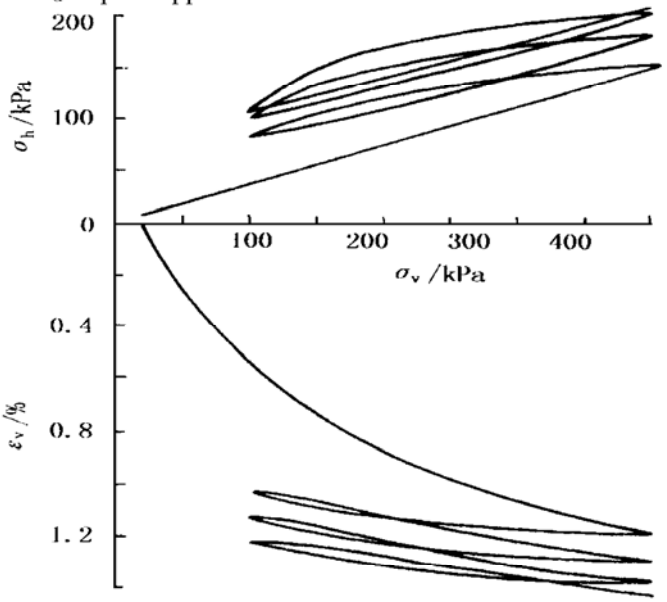

Fig. 13 Repeated one-dimensional compression

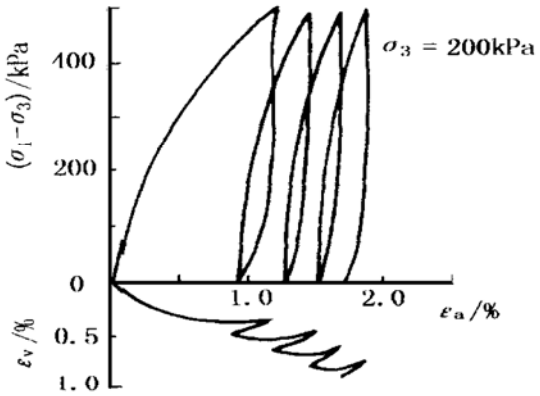

Fig. 14 Repeated drained triaxial test

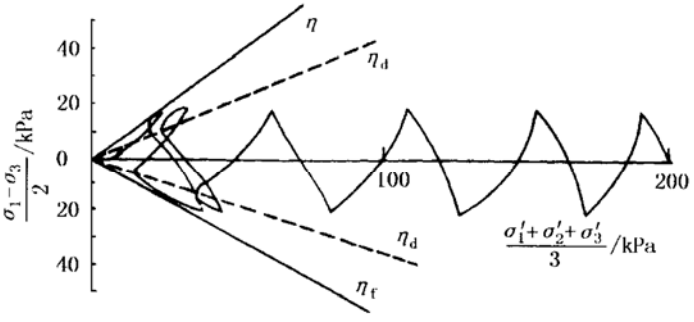

Fig. 15 Undrained cyclic triaxial test

4.3 Rotating stress path

Fig. 16 shows the simulated results of sand response to rotating stress path under constant η and drained condition. The vectors of strain increment clearly indicate their dependence on both the direction of total stress and the direction of stress increment. Fig. 17 shows the step-wise increase of volumetric strain because η increases when $\sigma_2 \rightarrow \sigma_1$ and decreases when $\sigma_2 \rightarrow \sigma_3$.

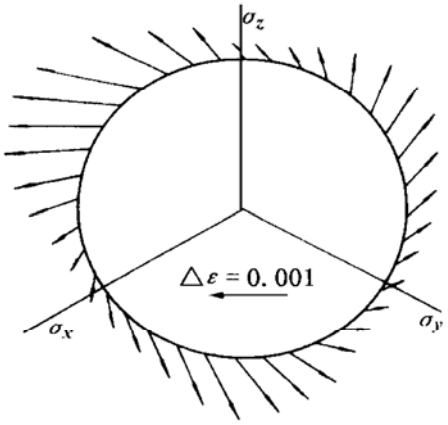

Fig. 16 Circular stress path in π plane

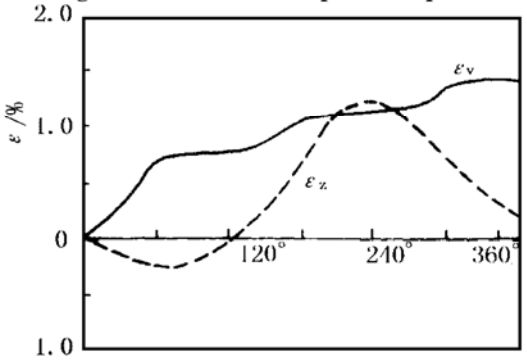

Fig. 17 Accumulations of strains under circular stress path

4.4 Rotation of principal stress axes

Now different values of η_f will be used, i.e. $\eta_{fM} = 0.62$ and $\eta_{fm} = 0.52$. Fig. 18 shows the results of simulation of rotation of principal stress axes. The pore pressure increases rapidly in first two cycles of rotation and then the fluctuation of pore pressure become more and more evident because stress ratio r increases when α increases from 0° to 90° and decreases when α changes oppositely.

Some experimental results which are aimed to be simulated can be found in references[12~14].

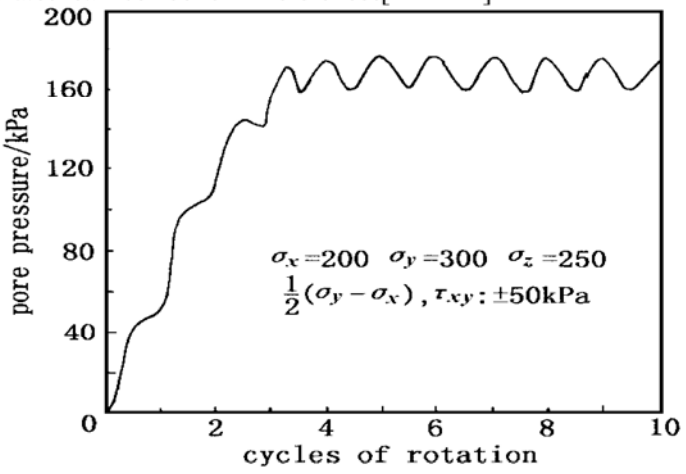

Fig. 18 Pore pressure buildup during stress axis rotation

5 Conclusions

(1) The model proposed in this paper is based on the understanding of mechanism of deformation behavior of granular material.

(2) Instead of using concept of yield function and plastic potential function which constitutes the main framework of classic theory of plasticity the proposed model assume the dependence of plastic strain upon the increment of stress tensor and the volumetric dilatancy is taken as recoverable deformation.

(3) The main constants entered in the model can be determined from conventional odometer test and triaxial compression test.

(4) The computed examples show that the proposed model can successfully simulate both drained and undrained responses of sand samples with different density under monotonous and complex loading, such as repeated and cyclic loading, turn of stress path and the rotation of principal stress axes.

References

1 Gutierrez M, Ishihara K and Towhata I. Model for the deformation of sands during rotation of principal stress direction. Soils & Foundations, 1993, **33**(3): 105~117

2 Matsuoka H and Sakakibara K. A constitutive model for sands and clays evaluating principal stress rotation. Soils and Foundations, 1987, **27**(4): 73~88

3 Wang Z L, Dafalias Y F and Shen C K. Bounding surface hypoplastic model for sand. J Eng Mech, ASCE, 1990, **116**(5): 983~1001

4 Bauer E and Wu W. A hypoplastic model for granular soil under cyclic loading. In: Proc Int Workshop on Modern Approach to Plasticity for Granular Materials. Norton, Greece, Elsevier, 1993. 247~258

5 Iai S, Matsunaga Y and Kameoka T. Strain space plasticity model for cyclic mobility. Soils & Foundations, 1992, **32**(2): 1~15

6 Oda M. Coordination numbers and its relation to shear strength of granular materials. Soils and Foundations, 1977, **17**(2): 32~42

7 Oda M, Konishi J and Nemat-Nasser S. Experimental micromechanical evaluation of the strength of granular materials-Effect of particle rolling. In: Edited by J T Jenkies & M Satake. Mechanics of Granular Materials. Elsevier, 1983. 9~19

8 Bhatia S K and Soliman A F. Frequency distribution of void ratio of granular materials determined by an imageanalyzer. Soils and Foundations, 1990, **30**(1): 1~16

9 Matsuoka H and Geka H. A stress-strain model for granular materials considering mechanism of fabric change. Soils and Foundations, 1983, **23**(2): 82~97

10 Tobita Y. Fabric tensors in constitutive equations for granular materials. Soils and Foundations, 1989, **29**(4): 91~104

11 Oda M, Korshikawa I and Higuchi T. Experimental study of anisotropical shear strength of sand by plane strain test. Soils and Foundations, 1978, **18**(1): 25~38

12 Nakata Y, Hyodo M, Murata H, et al. Flow deformation of sands subjected to principal stress rotation. Soils & Foundations, 1998, **38**(2): 115~128

13 Matsuoka H, Yamazaki H and Koyama H. A constitutive model of soils for estimating liquefaction resistance. In: 5th Int Conf Numerical Methods in Geomechanics. Nagoya, I. 381~388

14 沈瑞福等. 动主应力旋转下砂土孔隙压力发展及海床稳定性分析. 岩土工程学报, 1994, **16**(3): 70~78